

# Soil Arching Behind Retaining Walls under Active Translation Mode: Review and New Insights

M.H. Khosravi <sup>a, \*</sup>, M. Bahaaddini <sup>b</sup>, A.R. Kargar <sup>a</sup>, T. Pipatpongsa <sup>c</sup>

<sup>a</sup> School of Mining Engineering, College of Engineering, University of Tehran, Iran

<sup>b</sup> Shahid Bahonar University of Kerman, Iran

<sup>c</sup> Department of Urban Management, Kyoto University, Japan

## Article History:

Received: 18 August 2018,

Accepted: 27 September 2018,

Online: 13 November 2018.

## ABSTRACT

Granular materials have a tendency to exhibit an arching effect by which the load is transferred from yielding parts to adjacent stationary parts. Retaining walls are among those structures that the soil arching plays an important role in the distribution of earth pressures. This paper reviews briefly the development of soil arching theory and its application to different geotechnical projects. Various arching-based theoretical formulations for estimation of lateral active earth pressure on the rigid retaining walls were reviewed and their validity was examined through comparisons with the field data. It was concluded that, in spite of the conventional thought that the distribution of lateral earth pressure on the walls is linear, it is non-linear due to soil arching. Moreover, the maximum lateral stress does not appear at the toe of the wall; but it appears at some heights, leading to a shift of the point of application of thrust from 33% to approximately 40% of the wall height measured from the bottom of the wall.

**Keywords :** Arching effect, Soil arching, Retaining walls, Lateral earth pressure

## 1. Introduction

Arching effect is a phenomenon that has been used frequently by human being from ancient eras in engineering fields including architecture, geotechnics and mining. An ancient example of the application of arching effect in architecture is “Taq Kasra” vault, also called the “Archway of Ctesiphon”, constructed more than 2000 years ago during the Sasanian Persian Empire (Fig. 1). This vault, with a height of 37m and span of 26m, is considered as a landmark in the history of architecture and is the largest single-span vault of unreinforced brickwork in the world [1].



**Fig. 1.** “Taq Kasra” structure in Iraq constructed more than 2000 years ago during the Sasanian Persian Empire [1].

Arching effect can be observed in structures under both tensile and compressive stresses. A hanging chain is an example of structure under tensile stress where the shape of chain shows the trajectory of the major principal stress as illustrated in Fig. 2(a) [2]. An arch of blocks illustrated in Fig. 2(b) shows as arching effect in a structure under a compressive stress.

The aim of this paper is to review the phenomenon of arching in geomaterials with its application to different geotechnical projects with a focus on retaining walls.

## 2. Arching effect in geomaterial

If a localized area of a support yields for a mass of soil, the soil adjoining the yielding zone displaces while the rest of the soil remains stationary. In the transition zone between the moving and stationary soil masses, shear stresses are developed by the relative displacement of the two masses. Since the shearing resistance tends to maintain the yielding mass in its original position, the stress reorientation reduces the pressure on the yielding part of the support and increases the pressure on the adjoining stationary parts. This transfer of pressure from the yielding mass of soil onto the adjacent stationary parts is commonly called the arching effect, and the soil is said to arch over the yielding part of the support [3].

Generally, there are two types of arch actions in geo-materials: passive arch action, where trajectories of the major principal stress are continued, and active arch action, where trajectories of the minor principal stress are continued. The difference between these two types of arching is schematically illustrated in Fig. 3.

\* Corresponding author. E-mail address: [mh.khosravi@ut.ac.ir](mailto:mh.khosravi@ut.ac.ir) (M.H. Khosravi).

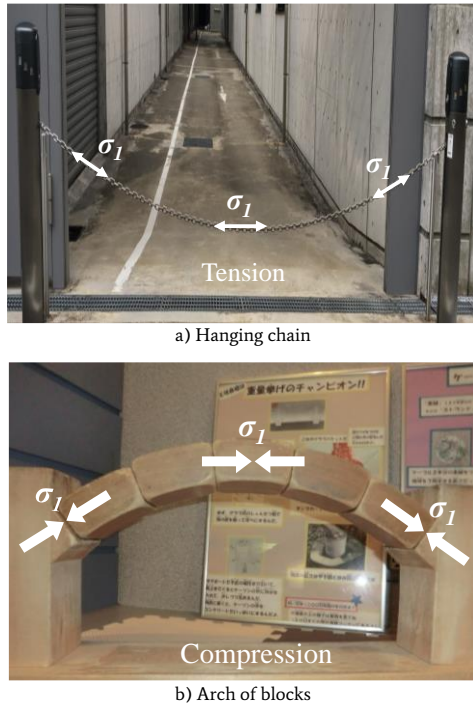


**Fig. 2.** Arching effect in structures under tensile and compressive stresses (Images by Thirapong Pipatpongsa: a) Katsura Campus, Kyoto University b) Akashi Kaikyo Bridge Exhibition Center, Japan).

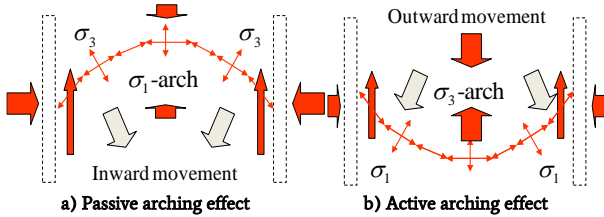


**Fig. 3.** Schematization of active and passive arching in geo-materials [4].

**2.1. Passive Arching Effect**

The well-known example of a passive arch action in geotechnical engineering exists in deep tunnels, where before digging the ground, the in-situ stresses are distributed inside the underground geo-materials in a certain condition. Suppose that the ground is initially in an active condition where the maximum principal stress,  $\sigma_1$ , is along the gravity direction and the minimum principal stress,  $\sigma_3$ , is in the transverse direction, normal to  $\sigma_1$  as shown in Fig. 4(a). By digging the ground and making an underground space, the condition of in-situ stresses disturbs. As illustrated in Fig. 4(b), the re-distribution of stresses is so that any free surface is a plane of the minimum principal stress. Therefore, the axes of the major principal stress orient and connect around the excavated area, which is referred to as a passive arch.

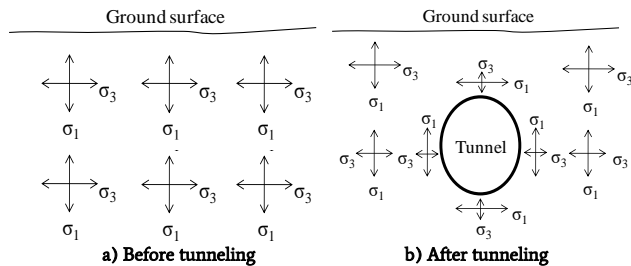


**Fig. 4.** Stress redistribution by tunneling.

The concept of passive soil arching has been also applied to pile stabilized slopes [5-9] as illustrated in Fig. 5. This application has

improved the estimation of optimum pile spacing to pile diameter ratio ( $s/d$ ), resulted in safer and more economical designs.

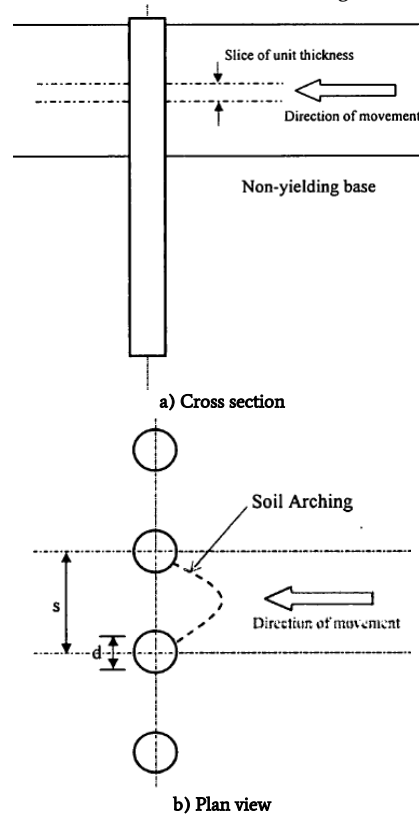


**Fig. 5.** Soil arching in pile stabilized slopes [8].

The passive soil arching in undercut slopes was studied through theoretical modeling [10], 1-g physical modeling [11-13], centrifugal modeling [14-16] and numerical modeling [17-19]. It was confirmed that an undercut slope could sustain its stability due to soil arching, as illustrated in Fig. 6. According to Pipatpongsa et al. (2009), the application of soil arching in undercut slope leads to a three dimensional slope analyses which gave a significant benefit in application of cut-and-fill mining, where side effects are considered to improve the stability of a finite slope [20]. Therefore, the passive arch action in undercut slopes should be considered in slope stability for safer and more economical designs of the slopes in open-pit mining, slopes of undercutting works in highways, etc. The concept of passive soil arching was adopted later for investigations on the performance of counterweight balance [21-22] and shear pins [23-25] on the stability of undercut slopes.

**2.2. Active Arching Effect**

The theory of active arching effect in granular materials is attributed to Janssen [26]. The vertical distribution of fluid pressure inside a silo is linear, confirming the hydrostatic condition, while it is nonlinear for a silo filled with bulk solids as illustrated in Fig. 7. This phenomenon of non-hydrostatic pressure in bulk solids is due to the interface friction between the bulk solids and the silo wall, known as “silo effect”. Many other researchers have also investigated the theoretical analysis of stresses in silos [27-30].

The concept of silo effect has been applied to some geotechnical works such as pipeline ditches, retaining walls, hoppers and earth slopes. Marston and Anderson [31] studied the effect of soil arching on vertical loads on pipes in earth ditches as illustrated in Fig. 8. They found that vertical loads on pipes reduce due to soil arching. Getzler et al. [32] modeled the soil arching above several buried structures and confirmed the findings of Marston and Anderson [31].

The equations developed by Marston and Anderson [31] were originally derived to define the boundary stresses in a backfilled trench, where the walls of the trench had a constant separation distance. The

backfill materials of the trench are partially supported by the friction of vertical walls (Fig. 9). Unlike a freestanding structural arch, where the trajectory of the major principal stress is continued, the arching that acts in partial support of bulk solids is represented by the trajectory of minor principal stress.

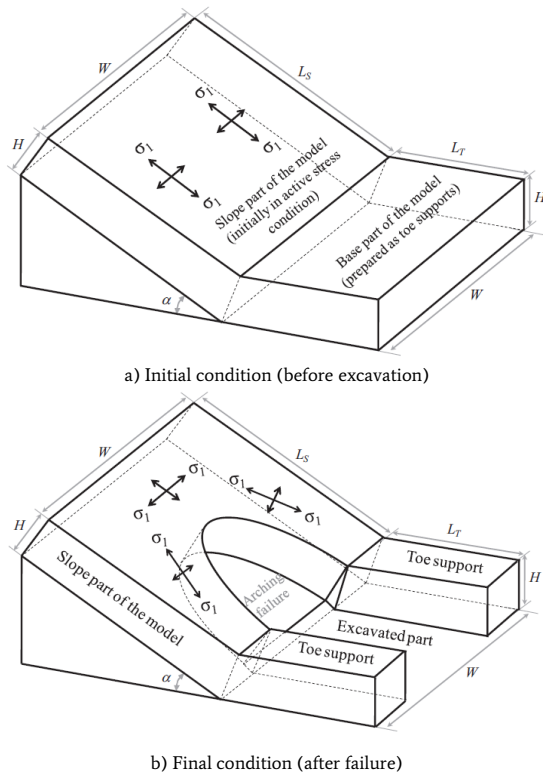


Fig. 6. Passive soil arching in undercut slopes [11].

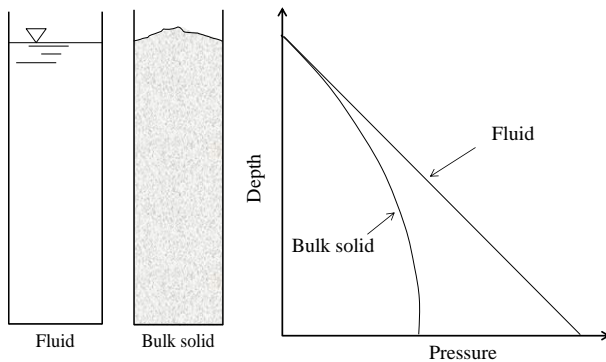


Fig. 7. The silo effect.

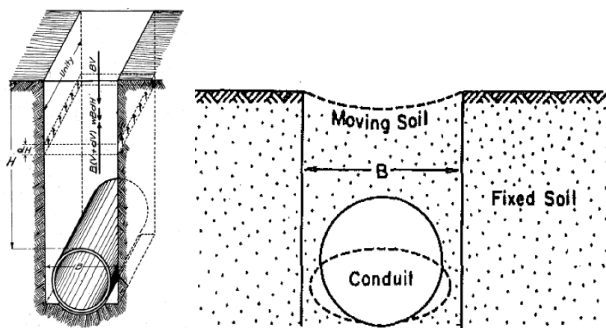


Fig. 8. Soil arching above a buried pipe (based on [31])

The weight of a flat horizontal element shown in Fig. 9 is partially supported by the side friction. The lateral stress is a product of the

vertical stress and a lateral stress ratio ( $K$ ). The value of  $K$  was obtained experimentally by Janssen [26] for grains, but later Marston and Anderson [31] assumed it equal to Rankine's [33] ratio of principal stresses with a level ground surface ( $K_r = \sigma_h / \sigma_v$ ). Many other researchers adopted this assumption, as well, while later it was found to be incorrect [34].

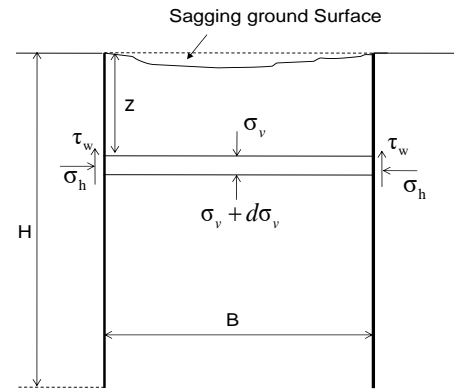


Fig. 9. Differential element in classical representation of soil arching in silos and trenches (based on [31]).

Krynine [34] found that by this assumption, the vertical and lateral stresses at the ends of a flat element (Fig. 9) must equal  $\sigma_1$  and  $\sigma_3$ , respectively, but  $\sigma_3$  is a principal stress that, by definition, must act on a plane of zero friction. This is a paradox and therefore, the assumption of Marston and Anderson [31] is not rigorous. The ratio of horizontal to vertical stresses at the wall ( $K_w = \sigma_h / \sigma_v$ ) was later derived by Krynine [34] as follows;

$$K_w = \frac{1 - \cos(\omega - \delta) \sin \phi}{1 + \cos(\omega - \delta) \sin \phi} \quad (1)$$

$$\omega = \sin^{-1} \left( \frac{\sin \delta}{\sin \phi} \right) \quad (2)$$

Where;

$K_w$ : Krynine's (1945) ratio of horizontal to vertical soil stress at the wall,

$\phi$ : internal friction angle of the backfill soil,

$\delta$ : interface friction angle.

For a fully rough wall,  $\delta = \phi$  and Krynine's stress ratio at the wall reduces to the following equation:

$$K_w = \frac{1 - \sin^2 \phi}{1 + \sin^2 \phi} \quad (3)$$

Thus, for a backfill material with the internal friction angle of  $\phi = 30^\circ$ , the lateral stress ratio at the wall is  $K_w = 0.60$  instead of  $K_r = 0.33$ , suggesting a fundamental reason that the use of  $K_r$  is unsafe for prediction of the lateral pressure in grain silos.

Walker [27] applied the concept of silo effect to hoppers. The main difference in analysis of hoppers, compared to silos with vertical walls, is that the width of the container varies with depth, making the analysis more complicated. Walker [27] concluded that in an ideal hopper, designed from the material strength-stress characteristics, walls should be smooth and get steeper towards the outlet.

Walters [35] extended his theoretical analysis of stresses from silos with vertical walls [28] to axially symmetric hoppers and bunkers. He studied the stress development due to arching during the initial filling of hoppers (static condition) and during the flow (dynamic condition). He derived a large switch stress during the change from static to dynamic conditions.

### 3. Soil arching behind retaining walls

Estimation of the lateral earth pressures acting against the retaining structures is essential in evaluating the performance of those structures. Conventionally, the active earth pressure against rigid walls was

calculated using either Coulomb's [36] or Rankine's [33] classical theories. While Coulomb's theory considers the forces acting on a failure wedge with a plane of rupture, Rankine's theory assumes that the distribution of lateral earth pressure against the wall is triangular and increases linearly with depth. However, many experimental results have shown that the distribution of active earth pressure on a wall is non-linear. The non-linearity of the active earth pressure distribution is resulted from arching effects in the backfill due to roughness of the retaining wall.

Terzaghi's observations [3] on the non-linear earth pressure distribution against the retaining walls can be considered as initial signs of soil arching in retaining structures. Without any analytical discussion on this phenomenon, Terzaghi [3] borrowed the concept of soil arching to explain the curvilinear distribution of lateral earth pressure against retaining walls.

Using Janssen's theory of soil arching, Handy [37] developed the initial elaborated analysis of arching behind rigid retaining walls under an active translation mode. He assumed a failure plane behind the wall under an active condition and developed his equations based on the integration of one-dimensional differential slices along the wall. His theory was later adopted by many researchers to improve the formulations using more sophisticated assumptions [38-44]. Moreover, many researches have been conducted on soil arching behind retaining walls through physical [45-50] and numerical modeling [51-53]. Some of the most important theories for estimation of the active earth pressure against rigid retaining walls are reviewed in this section and their estimations are evaluated against the field data in the following section.

**3.1. Handy (1985)**

Handy [37] applied the concept of soil arching to a single wall backfilled with a granular soil. He assumed a slip plane nominally inclined at  $\pi/4+\phi/2$  from the base of the wall. Along this plane, the principal stresses were oriented in vertical and horizontal directions, so the separation distance from the wall defined a half-arch as illustrated in Fig. 10(a). He stated that the trajectory of minor principal stress would approximate a catenary, where this catenary must be downward to support an active arch action.

Calculations of Handy [37] resulted in the following equation for estimation of the nonlinear active lateral earth pressure against the wall.

$$\sigma_h = \frac{\gamma}{\mu_w} H - z \tan\left(\frac{\pi - \phi}{4} - \frac{\phi}{2}\right) \left(1 - \exp\left(-\frac{\mu_w K_w}{\tan\left(\frac{\pi - \phi}{4} - \frac{\phi}{2}\right)} \frac{z}{H - z}\right)\right) \quad (4)$$

Where;

- $\gamma$ : unit weight of the backfill soil,
- $\mu_w$ : coefficient of wall friction,
- $H$ : height of retaining wall,
- $z$ : depth below the ground surface,

The analysis of Handy [37] showed that, for a rough wall, the soil arching initiated in two stages as illustrated in Fig. 10(b). During Stage I, the principal stresses rotate at the wall and make the earth pressure approximately higher than those predicted by classical theories. At its maximum development, it approximately equals Jaky's [54] expression for earth pressure at rest. If the wall's movement proceeds, the earth pressure on the wall reduces, particularly near the base of the wall. It results in a rounded rather than triangular earth pressure distribution on the wall.

**3.2. Wang (2000)**

Using the results of Coulomb's studies [36], Wang [39] assumed that the earth pressure against the wall is due to thrust exerted by a sliding wedge of soil between the wall and shear line, as shown in Fig. 11(a). A first-order differential equation was set up by considering the

equilibrium of the forces on an element of the sliding wedge illustrated in Fig. 11(b).

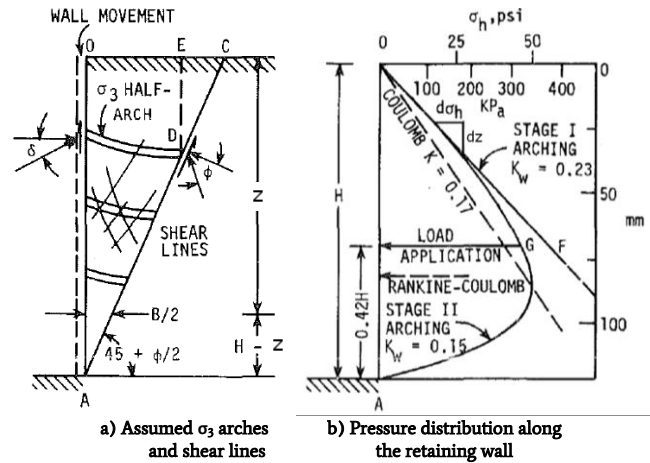


Fig. 10. Soil arching behind retaining walls [37].

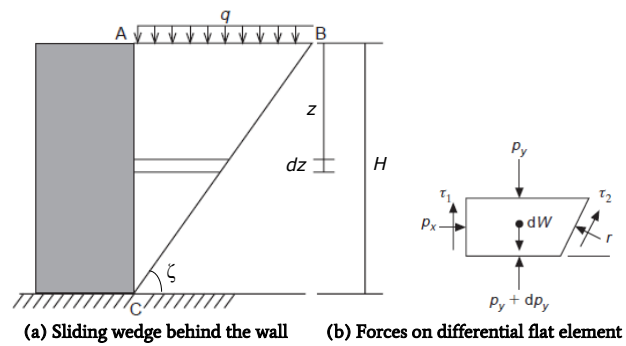


Fig. 11. Model of Wang [39].

Wang's formulation [39] resulted in estimation of the active lateral earth pressure against a retaining wall:

$$\sigma_h = K \left[ \left( q - \frac{\gamma H}{aK - 2} \right) \left( \frac{H - z}{H} \right)^{aK - 1} + \frac{\gamma H}{aK - 2} \left( \frac{H - z}{H} \right) \right] \quad (5)$$

$$a = \frac{\cos \zeta - \phi - \delta \tan \zeta}{\sin \zeta - \phi \cos \delta} \quad (6)$$

Where;

$K$ : lateral earth pressure coefficient which should be between the active earth pressure coefficient  $K_a$  and the coefficient  $K_0$  of earth pressure at rest,

$q$ : uniform surcharge on the retained soil.

It is noticeable that the parameter  $a$  corresponding to the critical inclination of shear line, which yields the maximum resultant pressure on the wall, is related to the active earth pressure coefficient  $K_a$  of Coulomb's theory by the following equation:

$$a = \frac{1}{K_a \cos \delta} \quad (7)$$

$$K_a = \frac{\cos^2 \phi}{\cos \delta \left( 1 + \sqrt{\frac{\sin \phi + \delta \sin \phi}{\cos \delta}} \right)^2} \quad (8)$$

The lateral active force on the wall ( $P_a$ ) and the application height of the lateral active force ( $h_a$ ) can be calculated from the following equations:

$$P_{aH} = \frac{\sin\left(\frac{\pi - \phi}{4} - \frac{\phi}{2}\right) \cos \delta \cot\left(\frac{\pi + \phi}{4} + \frac{\phi}{2}\right)}{\cos\left(\frac{\pi - \phi}{4} - \delta\right)} \left( qH + \frac{1}{2} \gamma H^2 \right) \quad (9)$$

$$h_a = \left[ \frac{1}{3} + \frac{aK - 1}{3(aK + 1)} \right] H \frac{3q + \gamma H}{2q + \gamma H} \quad (10)$$

### 3.3. Paik and Salgado (2003)

Paik and Salgado [40] adapted Walker's [27] method of stress solution of hoppers for estimation of the earth pressure on rigid retaining walls under an active translation mode. They assumed a circular trajectory for minor principal stress with the radius  $R$  and the constant major principal stress  $\sigma_1$  along the arch as shown in Fig. 12.

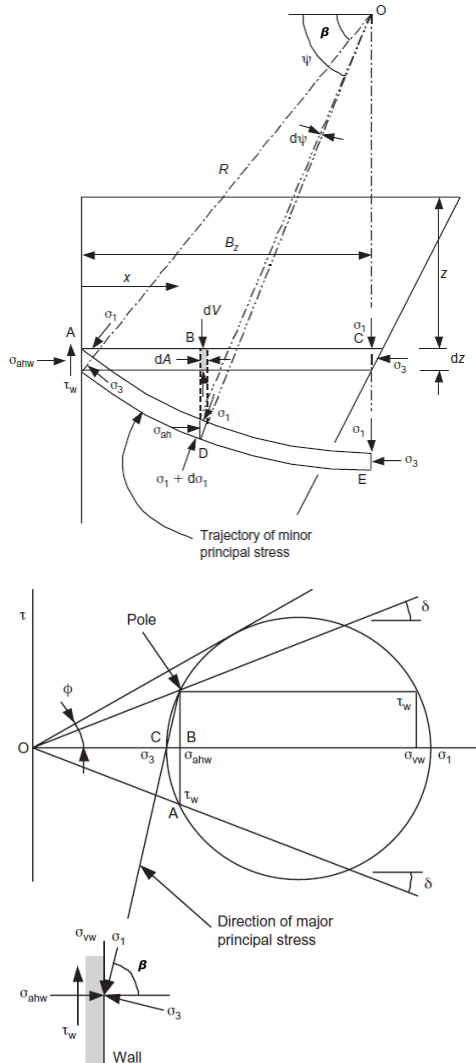


Fig. 12. Stresses on a differential flat element in backfill and Mohr circle for stresses at the wall [40].

The direction of the major principal stress at the wall was inclined with an angle  $\beta$ .

$$\beta = \tan^{-1} \left( \frac{(N - 1) \pm \sqrt{(N - 1)^2 - 4N \tan^2 \delta}}{2 \tan \delta} \right) \quad (11)$$

where  $N$  is the ratio of major to minor principal stresses,  $N = \tan^2 \pi/4 + \phi/2$

Based on these assumptions, a new active lateral stress ratio at the wall ( $K_{avn}$ ) was defined in the following form:

$$K_{avn} = \frac{3(N \cos^2 \beta + \sin^2 \beta)}{3N - (N - 1) \cos^2 \beta} \quad (12)$$

Their assumed that the rectangular differential flat element is

subjected to stresses shown in Fig. 13.

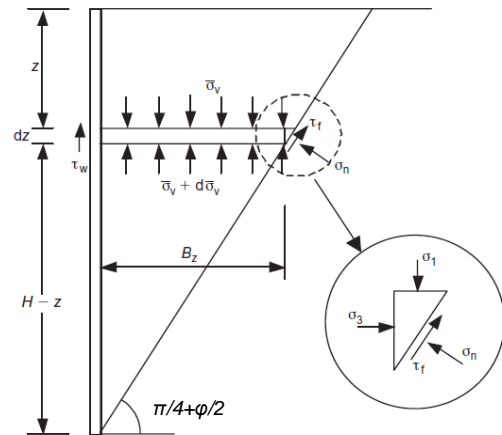


Fig. 13. Free body diagram of differential flat element with a linear shear surface [40].

By taking equilibrium in vertical direction, the active lateral earth pressure against the wall can be obtained from the following equation:

$$\sigma_h = \frac{\gamma H K_{avn}}{1 - K_{avn} \tan \delta \tan \left( \frac{\pi}{4} + \frac{\phi}{2} \right)} \left( \left( \frac{H-z}{H} \right)^{K_{avn} \tan \delta \tan \left( \frac{\pi}{4} + \frac{\phi}{2} \right)} - \left( \frac{H-z}{H} \right) \right) \quad (13)$$

The lateral active force normal to the wall ( $P_{ah}$ ) and the application height of the lateral active force ( $h_a$ ) on the wall can be calculated from the following equations, respectively:

$$P_{ah} = \frac{\gamma H^2}{2} \frac{K_{avn}}{1 + K_{avn} \tan \delta \tan \left( \frac{\pi}{4} + \frac{\phi}{2} \right)} \quad (14)$$

$$h_a = \frac{2 \left( 1 + K_{avn} \tan \delta \tan \left( \frac{\pi}{4} + \frac{\phi}{2} \right) \right)}{3 \left( 2 + K_{avn} \tan \delta \tan \left( \frac{\pi}{4} + \frac{\phi}{2} \right) \right)} H \quad (15)$$

### 3.4. Khosravi et al. (2016)

So far, all of the reviewed methods were based on one-dimensional system of equilibrium along the wall assuming a differential flat element between the wall and the slip line behind the wall. Therefore, all of those methods could predict the stress distribution only along the wall and the stress distribution in the failure zone behind the wall remained unknown.

Khosravi et al. [42] extended their calculations to two-dimensional system of equilibrium as illustrated in Fig. (14). They adopt the assumption of a uniform vertical stress in any horizontal plane, previously used in two-dimensional silo problems, to derive stress solutions in a rectangular coordinate system.

Equations for vertical, horizontal and shear stresses in the failure wedge between a rigid retaining wall under the active translation mode and the stationary soil are proposed as follows:

$$\sigma_z(z) = \frac{\gamma H}{1-n} \left[ \left( \frac{H-z}{H} \right)^n - \frac{H-z}{H} \right] + q \left( \frac{H-z}{H} \right)^n \quad (16)$$

$$\sigma_x(x, z) = \left( K_w - n^2 \tan \left( \frac{\pi}{4} + \frac{\phi}{2} \right) \frac{x}{H-z} + \frac{n-1}{2} n \left( \frac{x}{H-z} \right)^2 \right) \sigma_z(z) + \frac{n\gamma x}{2} \left( 2 \tan \left( \frac{\pi}{4} + \frac{\phi}{2} \right) - \frac{x}{H-z} \right) \quad (17)$$

$$\tau_{xz}(x, z) = n \left( \tan \left( \frac{\pi}{4} + \frac{\phi}{2} \right) - \frac{x}{H-z} \right) \sigma_z(z) \quad (18)$$

Where  $n = \mu_w K_w / \tan(\pi/4 + \phi/2)$ .

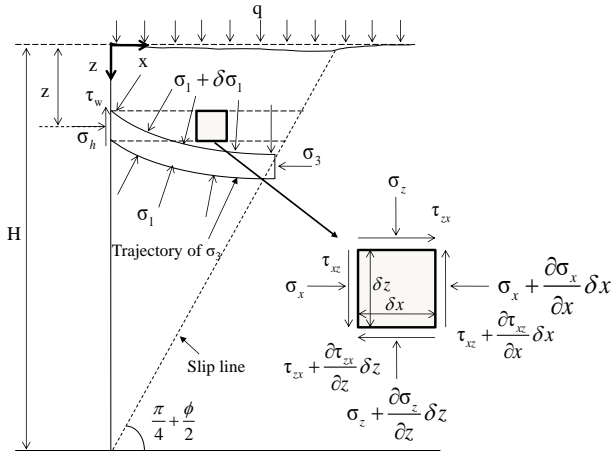


Fig. 14. Free body stress diagram of a differential element of backfill soil with a linear shear surface [42].

Contours of stress distributions obtained from the proposed equations behind the retaining wall are plotted in Fig. 15. In this example, the wall height is  $H = 1$  m, the soil properties are  $\phi = \delta = 35^\circ$ ,  $c = 0$  kPa,  $\gamma = 14$  kN/m<sup>3</sup> and no surcharge is existing on the backfill soil. The distribution of principal stresses inside the failure wedge for the same retaining wall is shown in Fig. 16. It is noteworthy that the principal directions coincide with vertical and horizontal directions on the shear line while they rotate by getting closer to the wall, reaching their maximum rotation on the wall.

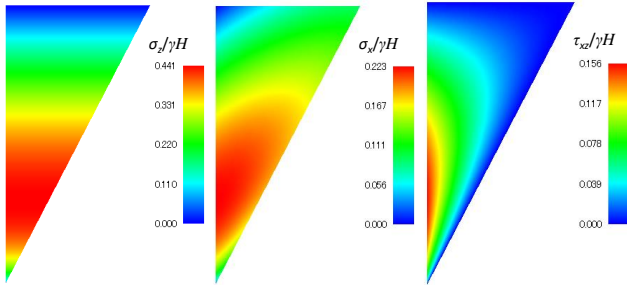


Fig. 15. Distribution of stresses inside the failure wedge behind a rough rigid retaining wall under an active translation mode [42].

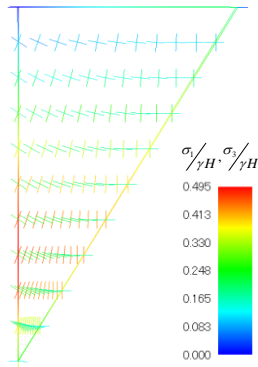


Fig. 16. Principal stresses in the failure wedge behind a rough rigid retaining wall under an active translation mode [42].

Substituting  $x=0$  in Eq. (17) results the following equation for the distribution of the lateral earth pressure at the wall.

$$\sigma_h = \frac{\gamma H K_w}{1-n} \left[ \left( \frac{H-z}{H} \right)^n - \frac{H-z}{H} \right] + q \left( \frac{H-z}{H} \right)^n \quad (19)$$

The lateral active force normal to the wall ( $P_{ah}$ ) and the application height of the lateral active force ( $h_a$ ) on the wall can be calculated from the following equations, respectively:

$$P_{ah} = \frac{K_w H}{n+1} \left( \frac{\gamma H}{2} + q \right) \quad (20)$$

$$h_a = \frac{2(n+1)}{3(n+2)} \left( \frac{\gamma H + 3q}{\gamma H + 2q} \right) H \quad (21)$$

### 3.5. Xie and Leshchinsky (2016)

So far, in the development of closed-form equations for estimation of the earth pressure against the retaining wall, the shear surface behind the wall was assumed to be planar. However, the observed shear surface that often develops in retaining structures is non-planar. Moreover, previous arching-based researches have primarily focused on a vertical retaining wall, while a batter (wall inclination) is frequently applied in actual retaining structures.

In order to cover the above-mentioned limitations in previous studies, Xie and Leshchinsky [43] considered both the log-spiral failure mechanism and wall inclination in their analysis (Fig. 17). However, their analysis was limited to the earth pressure distribution only on the wall.

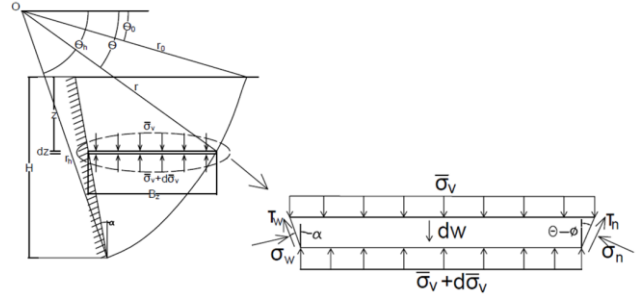


Fig. 17. Free body stress diagram of a differential flat element of backfill soil with a log-spiral shear surface [43].

The trajectory of principal stresses along an inclined retaining wall and the Mohr circle represents the stress conditions at the wall are shown in Fig. 18.

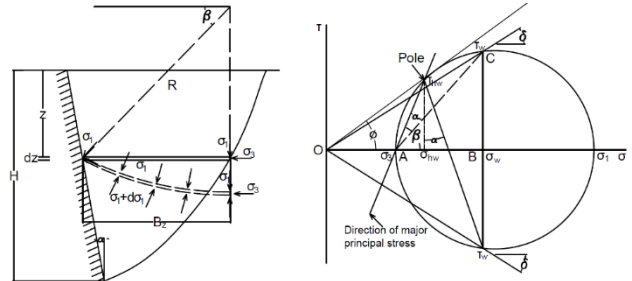


Fig. 18. Stresses on differential flat element in backfill and Mohr circle for stresses at the wall [43].

Xie and Leshchinsky [43] calculations resulted in a first-order differential equation, which was solved numerically using a finite-difference scheme. Subsequently, they derived an equation for lateral earth pressure against the wall with a batter of  $\alpha$  as:

$$\sigma_n = \sigma_1 \cos^2(\beta - \alpha) + \sigma_3 \sin^2(\beta - \alpha) \frac{\cos(\alpha + \delta)}{\cos \delta} \quad (22)$$

Where  $\sigma_1$  and  $\sigma_3$  are major and minor principal stresses obtained numerically, and the parameter  $\beta$  is determined as follows:

$$\beta = \tan^{-1} \left( \frac{(N-1) \pm \sqrt{(N-1)^2 - 4N \tan^2 \delta}}{2 \tan \delta} \right) + \alpha \quad (23)$$

Furthermore, for a given or assumed  $\theta_0$  and  $\theta_h$ , the lateral active force normal to the wall ( $P_a$ ) can be calculated by integrating lateral earth pressures over the height of the wall.

$$P_{ah} = \int_0^H \sigma_n dz \quad (24)$$

The application height of the lateral active force ( $h_a$ ) on the wall can

be calculated from the following equation where  $M$  is the moment about the wall base.

$$h_a = \frac{M}{P_a} \tag{25}$$

**3.6. Khosravi et al. (2018)**

Two common types of non-linear failure curves, parabolic and log-spiral, are investigated by Khosravi et al. [44]. The curvature of the slip surface was defined by a new parameter, namely “planar ratio of slip surface” ( $R_{pl}$ ) as illustrated in Fig. 19.

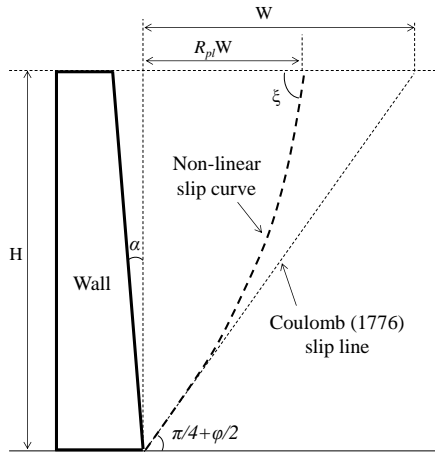


Fig. 19. Non-linear slip curve behind the retaining wall [44].

For a log-spiral failure surface the ratio  $R_{pl}$  can be calculated from the following equation.

$$R_{pl} = -\frac{1}{\tan\left(\frac{\pi - \varphi}{4}\right)} \frac{\cos\left(\frac{\pi}{2} + \varphi - \xi\right) - e^{\left(\xi - \frac{\pi}{4} - \frac{\varphi}{2}\right)\tan\varphi} \cos\left(\frac{\pi}{4} + \frac{\varphi}{2}\right)}{\sin\left(\frac{\pi}{2} + \varphi - \xi\right) - e^{\left(\xi - \frac{\pi}{4} - \frac{\varphi}{2}\right)\tan\varphi} \sin\left(\frac{\pi}{4} + \frac{\varphi}{2}\right)} \tag{26}$$

Where  $\xi$  is the inclination of the slip curve at the top of the wall. The inclination of the failure surface at the toe was assumed to be a constant value of  $\pi/4 + \varphi/2$ .

The ratio  $R_{pl}$  ranges from 1 ( $\xi = \pi/4 + \varphi/2$ , planar failure surface) to  $R_{pl}^*$  ( $\xi = \pi/2$ , the maximum possible curvature of a log-spiral failure surface).

$$R_{pl}^* = -\frac{1}{\tan\left(\frac{\pi - \varphi}{4}\right)} \frac{\cos\varphi - e^{\left(\frac{\pi}{4} - \frac{\varphi}{2}\right)\tan\varphi} \cos\left(\frac{\pi}{4} + \frac{\varphi}{2}\right)}{\sin\varphi - e^{\left(\frac{\pi}{4} - \frac{\varphi}{2}\right)\tan\varphi} \sin\left(\frac{\pi}{4} + \frac{\varphi}{2}\right)} \tag{27}$$

Similarly, for a parabolic failure surface the ratio  $R_{pl}$  can be calculated from the following equation.

$$R_{pl} = \left(1 + \frac{\tan\beta - \tan\left(\frac{\pi}{4} + \frac{\varphi}{2}\right)}{2 \tan^2\left(\frac{\pi}{4} + \frac{\varphi}{2}\right) \tan\left(\frac{\pi}{4} - \frac{\varphi}{2}\right)}\right)^{-1} \tag{28}$$

Where,  $R_{pl}$  ranges from 1 ( $\xi = \pi/4 + \varphi/2$ , planar failure surface) to zero ( $\xi = \pi/2$ ), mathematically. However, note that as  $R_{pl}$  approaches to zero, the failure wedge behind the wall diminishes, which has no physical meaning.

By increasing  $R_{pl}$ , the difference between log-spiral and parabolic failure surfaces reduces where by approaching  $R_{pl}$  to unity, both log-spiral and parabolic failure surfaces reduces to a planar failure surface.

A free-body stress diagram of a differential element of backfill soil with reference axis at the upper surface of the yielding zone is illustrated

in Fig. 20.

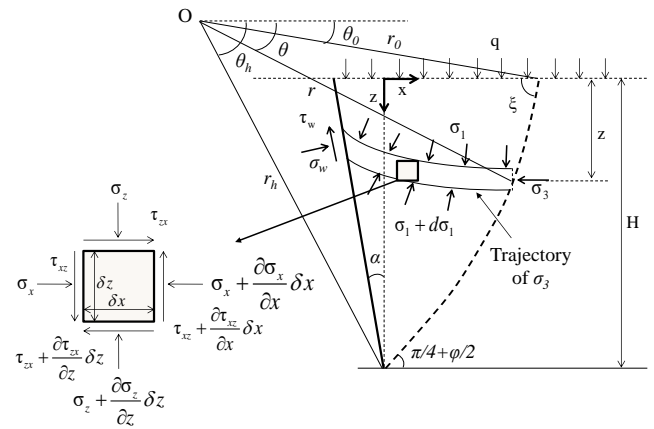


Fig. 20. Free-body stress diagram of a differential element of backfill soil [44].

Khosravi et al. [44] calculations resulted in a second-order differential equation, which was solved numerically using a finite-difference scheme. The following equations were derived for vertical, horizontal and shear stresses in the failure zone between a rigid retaining wall under active translation mode and log-spiral failure curve, respectively.

$$\sigma_{z \ i+1} = \sigma_{z \ i} + \Delta z \left[ \gamma - \frac{K_w \sigma_{z \ i}}{r_0 e^{(\theta_i - \theta_0) \tan \varphi} \cos \theta_i - r_0 e^{\left(\frac{\pi}{4} + \frac{\varphi}{2} - \theta_0\right) \tan \varphi} \cos\left(\frac{\pi}{4} + \frac{\varphi}{2}\right) - \tan \alpha (z_{(\theta_i)} - H)} \right] \tag{29}$$

$$\sigma_{x \ i, j+1} = \sigma_{x \ i, j} - \frac{\Delta x}{\Delta z} (\tau_{xz \ i+1, j} - \tau_{xz \ i, j}) \tag{30}$$

$$\tau_{xz \ i, j} = -K_w \sigma_{z \ i} \left[ 1 + \frac{\tan \alpha (z_{(\theta_i)} - H) - x_j}{r_0 e^{(\theta_i - \theta_0) \tan \varphi} \cos \theta_i - r_0 e^{\left(\frac{\pi}{4} + \frac{\varphi}{2} - \theta_0\right) \tan \varphi} \cos\left(\frac{\pi}{4} + \frac{\varphi}{2}\right) - \tan \alpha (z_{(\theta_i)} - H)} \right] \tag{31}$$

Where the indices  $i$  and  $j$  denote the number of nodes in vertical and horizontal directions, respectively.

The ratio of shear stress to vertical stress along the wall ( $K_w$ ) is evaluated according to the following equation, where  $\beta$  can be calculated from Eq. (20).

$$K_w = \frac{\sin \varphi \sin 2\beta}{(1 + \sin \varphi) \sin^2 \beta + (1 - \sin \varphi) \cos^2 \beta} \tag{32}$$

Similarly, for a parabolic failure curve, the following equations were derived.

$$\sigma_{z \ i+1} = \sigma_{z \ i} + \Delta z \left[ \gamma + \frac{2aK_w \sigma_{z \ i}}{b + \left(b^2 - 4a(c - z_i)\right)^{\frac{1}{2}} + 2a \tan \alpha (z_i - H)} \right] \tag{33}$$

$$\sigma_{x \ i, j+1} = \sigma_{x \ i, j} - \frac{\Delta x}{\Delta z} (\tau_{xz \ i+1, j} - \tau_{xz \ i, j}) \tag{34}$$

$$\tau_{xz \ i, j} = -K_w \sigma_{z \ i} \left[ 1 - \frac{2a\tau_w}{b + \left(b^2 - 4a(c - z_i)\right)^{\frac{1}{2}} + 2a \tan \alpha (z_i - H)} \right] \tag{35}$$

The stress distribution inside the backfill soil ( $\phi = 35^\circ$ ) behind a rough vertical wall ( $\delta = 0.8$ ,  $\phi = 0^\circ$ ) with a height of  $H = 10$  m and uniform surcharge of  $q = 0.1 \gamma H$ , for both log-spiral and parabolic failure surfaces are illustrated in Figs. 21 and 22, respectively. The stress values shown in these figures are normalized by  $\gamma H$ .

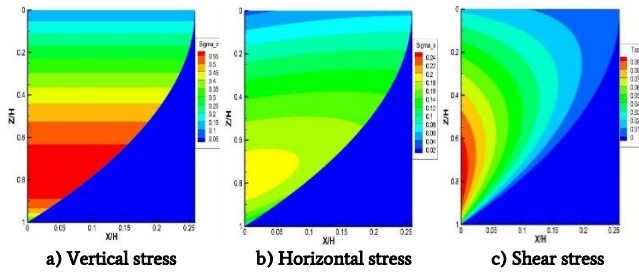


**Fig. 21.** Normalized stresses inside the backfill soil with a log-spiral failure surface behind a vertical retaining wall under active translation mode [44].

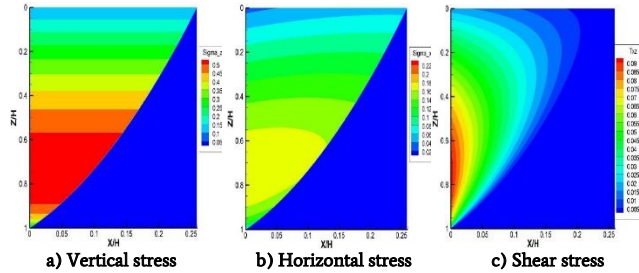


**Fig. 22.** Normalized stresses inside the backfill soil with a parabolic failure surface behind a vertical retaining wall under active translation mode [44].

The resultant lateral active force ( $P_{ah}$ ) on the wall can be obtained by integrating the equations of horizontal stress with respect to  $z$  at the wall ( $\Omega$ ):

$$P_{ah} = \int_0^H \sigma_x(x, z) \Big|_{\Omega} dz \tag{36}$$

In addition, the application height of the resultant lateral active force ( $h_a$ ) can be obtained using the following equation:

$$h_a = \frac{M_{ah}}{P_{ah}} \tag{37}$$

Where  $M_{ah}$  is the moment of the horizontal stress about the base of the wall:

$$M_{ah} = \int_0^H \sigma_x(x, z) \Big|_{\Omega} (H - z) dz \tag{38}$$

#### 4. Result and discussion

In order to evaluate the ability of different theoretical methods in estimation of lateral earth pressure distribution, the field measurement of Tsagareli [45] were employed and the results are depicted in Fig. 23. Although Coulomb's active wedge solution is originally expressed in terms of force, a linear pressure distribution with the depth is assumed along a wall, as shown in this figure. Moreover, the magnitude of the lateral active force and the height of application point of the lateral active force are compared in Fig. 24 and Fig. 25, respectively. The soil properties in Tsagareli's experiments were  $\phi = \delta = 37^\circ$  and  $\gamma = 17.65 \text{ kN/m}^3$ .

The results show that the equations of Handy [37], Wang [39], and Xie and Leshchinsky [43] underestimate the active lateral pressure against the wall. Other arching-based equations show good agreements with experimental data. Khosravi et al.'s formulation [42] was developed for a two-dimensional stress analysis covering the wedge zone between the wall and the stationary soil behind the planar slip surface. This formulation released a lateral active earth pressure close to that of Paik and Salgado's [40] at the wall, as illustrated in Fig. 23. Khosravi et al.'s formulation [42] was extended later to cover a range of slip surfaces from planar to log-spiral and parabolic non-planar slip surfaces, by defining a new so called "planar ratio of slip surface" parameter,  $R_{pl}$  [44]. Their results showed that as  $R_{pl}$  increased, the two defined non-planar slip curves converged together so that for  $R_{pl}$  values more than 0.8, the log-spiral and parabolic slip curves coincided. Moreover, for  $R_{pl}$  values equal to one, non-linear slip curves reduced to Coulomb's slip line [36].

Since  $R_{pl}$  values of Tsagareli's experiments [45] are more than 0.8, the resultant earth pressure distributions predicted by non-planar slip surfaces shown in Fig. 23 coincide and approximately touch the predictions from planar slip surfaces of Paik and Salgado [40], and Khosravi et al. [42].

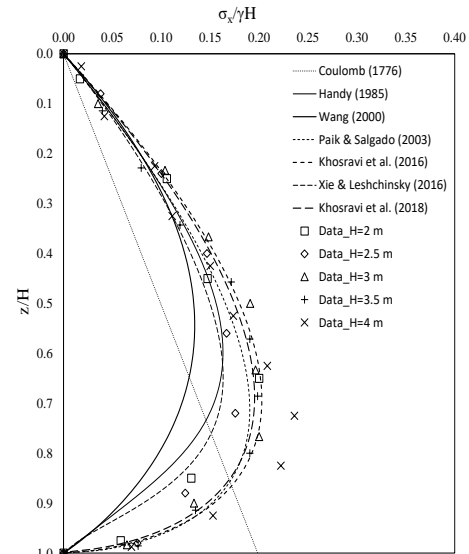


**Fig. 23.** Theoretical predictions for the distributions of horizontal active stress compared with full-scale measurements (Data from Tsagareli [45]).

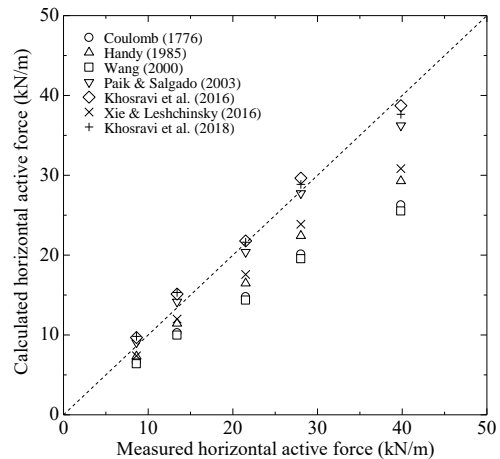


**Fig. 24.** Theoretical predictions for the magnitude of lateral active force compared with full-scale measurements (Data from Tsagareli [45]).

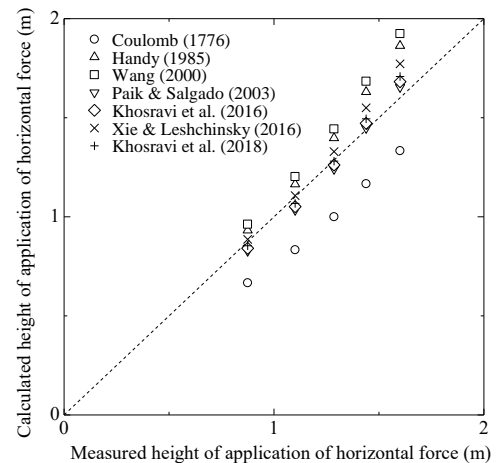


**Fig. 25.** Theoretical predictions for the height of application point of the lateral active force compared with full-scale measurements (Data from Tsagareli [45]).

The results of all arching-based formulations confirmed Terzaghi's findings [3] that the lateral earth pressure against the retaining wall is non-linear. Therefore, as shown in Fig. 25, the linear earth pressure distribution assumed by Rankine [33] and Coulomb [36] underestimates the height of application point of the lateral active force. Due to soil arching, the lateral earth pressure increases at the upper portion of the wall while decreases at the lower portion, as shown schematically in Fig. 26. Therefore, the total thrust on the wall is not necessarily at a height of  $0.33H$ , as suggested by classical theories of Rankine [33] and Coulomb [36], but it is at a height of about  $0.40H$ .

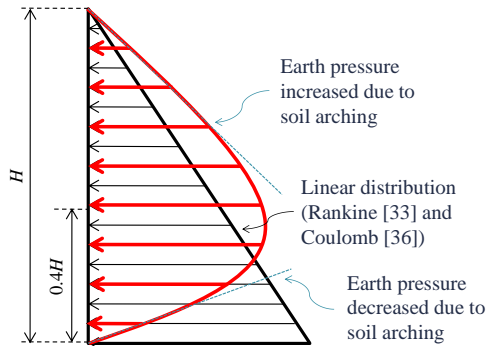


Fig 26. The influence of soil arching on the lateral earth pressure against retaining walls under an active translation mode.

## 5. Conclusions

In this paper, various formulations, which have been developed based on soil arching, were reviewed to estimate the lateral active earth pressure, acting against a rigid retaining wall under active translation mode. The developed equations were compared with Coulomb's classical theory [36] as well as some field data. The results of all arching-based formulations confirmed that the lateral earth pressure acting against the retaining walls under an active translation mode is non-linear. Therefore, the total thrust on the wall is located at a height more than what predicted by classical theories leading to a higher overturning moment. Furthermore, it was concluded that the assumption of a planar slip surface could be acceptable for shallow retaining walls. However, according to the experimental data, as the wall's height increase, the curvature of the slip surface increases, as well.

## REFERENCES

- [1] Taq Kasra (2018), from Wikipedia, the free encyclopedia.
- [2] Khosravi, M. H. (2012). Arching effect in geomaterials with applications to retaining walls and undercut slopes. Ph.D. dissertation. Tokyo Institute of Technology, Tokyo, Japan.
- [3] Terzaghi, K. (1934). Large retaining-wall tests. Engineering News-Record, McGraw-Hill.
- [4] Pipatpongsa, T., Khosravi, M. H., Leelasukseree, C., Mavong, N., and Takemura, J. (2010). Slope failures along oblique plane due to sequential removals of propping portion in physical model tests. The 15th National Convention on Civil Engineering, GTE60, Ubon Ratchathani, Thailand.
- [5] Ito, T., Matsui, T., and Hong, W. P. (1981). Design method for stabilizing piles against landslide-one row of piles, Soils and Foundations, March, Vol.21, No.1, pp. 21-37.
- [6] Bosscher, P. J. and Gray, D. H. (1986). Soil arching in sandy slopes. Journal of Geotechnical Engineering, 112(6), 626-645.
- [7] Adachi, T., Kimura, M., and Tada, S. (1989). Analysis on the preventive mechanism of landslide stabilizing piles. Numerical Models in Geomechanics, 15(3), 691-698.
- [8] Liang, R.Y. and Zeng, S. (2002). Numerical study of soil arching mechanism in drilled shafts for slope stabilization. Soils and Foundations, 42(2), 83-92.
- [9] Chen C Y and Martin G R (2002) Soil-structure interaction for landslide stabilizing piles, Computers and Geotechnics, Vol. 29, 363-386.
- [10] Khosravi, M. H., Pipatpongsa, T., and Takemura, J. (2012). Pseudo-static analysis of passive arch action in undercut slopes against earthquake. The 9th International Conference on Urban Earthquake Engineering, Tokyo, Japan.
- [11] Khosravi, M. H., Pipatpongsa, T., Takahashi, A., and Takemura, J. (2011). Arch action over an excavated pit on a stable scarp investigated by physical model tests. Soils and Foundations, 51(4), 723-35.
- [12] Pipatpongsa, T., Khosravi, M. H., and Takemura, J. (2013). Physical modeling of arch action in undercut slopes with actual engineering practice to Mae Moh open-pit mine of Thailand. The 18th International Conference on Soil Mechanics and Geotechnical Engineering, Paris, France.
- [13] Pipatpongsa, T., Khosravi, M. H., Takemura, J., and Leelasukseree, C. (2016). Modelling concepts of passive arch action in undercut slopes. The First Asia Pacific Slope Stability in Mining Conference, Perth, Australia.
- [14] Khosravi, M. H., Takemura, J., and Pipatpongsa, T. (2013). Centrifugal modeling of undercut slopes subjected to pseudo-static loading. The 10th International Conference on Urban Earthquake Engineering, Tokyo, Japan.
- [15] Khosravi, M. H., Takemura, J., Pipatpongsa, T., and Amini, M. (2016). In-flight Excavation of Slopes with Potential Failure Planes. Journal of Geotechnical and Geoenvironmental Engineering, doi:10.1061/(ASCE)GT.1943-5606.0001439.
- [16] Khosravi, M. H., Pipatpongsa, T., Takemura, J., and Amini, M. (2017). Influence of modeling material on undercut slope failure mechanism. Journal of Mining and Environment 8 (4), 645-662.
- [17] Leelasukseree, C., Khosravi, M. H., Pipatpongsa, T., and Mavong, N. (2010). Investigation of load transfer mechanisms due to undercutting at toe of slope resting on sliding plane by using 3D elastic analyses. The 12th JSCE International Summer Symposium, Tokyo, Japan.
- [18] Leelasukseree, C., Pipatpongsa, T., Khosravi, M. H., and Mavong, N. (2012). Stresses and a failure mode from physical and numerical models of undercut slope lying on inclined bedding plane. ISRM Regional Symposium-7th Asian Rock Mechanics Symposium, Seoul, Korea.
- [19] Ukritchon, B., Ouch, R., Pipatpongsa, T., and Khosravi, M. H. (2018). Investigation of stability and failure mechanism of undercut slopes by three-dimensional finite element analysis. KSCE Journal of Civil Engineering 22(5), 1730-1741.
- [20] Pipatpongsa, T., Khosravi, M. H., Doncommul, P., and Mavong, N. (2009). Excavation problems in Mae Moh lignite open-pit mine of Thailand. The Japanese Geotechnical Society, Tohigi, Japan.
- [21] Khosravi, M. H., Tang, T., Pipatpongsa, P., Takemura, J., and Doncommul, P. (2012). Performance of counterweight balance on stability of undercut slope evaluated by physical modeling. International Journal of Geotechnical Engineering, 6, 193-205.
- [22] Khosravi, M. H., Sarfaraz, H., Esmailvandi, M., and Pipatpongsa, T. (2017). A Numerical Analysis on the Performance of Counterweight Balance on the Stability of Undercut Slopes. International Journal of Mining and Geo-Engineering 51 (1), 63-69.

- [23] Ukritchon, B., Ouch, R., Pipatpongsa, T., and Khosravi, M. H. (2017). Experimental studies of floor slip tests on soil blocks reinforced by brittle shear pins. *International Journal of Geotechnical Engineering*, DOI: 10.1080/19386362.2017.1314126
- [24] Ouch, R., Ukritchon, B., Pipatpongsa, T., and Khosravi, M. H. (2017). Finite element analyses of the stability of a soil block reinforced by shear pins. *Geomechanics and Engineering* 12 (6), 1021-1046.
- [25] Ouch, R., Ukritchon, B., Pipatpongsa, T., and Khosravi, M. H. (2018). Experimental investigations of shear pin arrangement on soil slope resting on low interface friction plane. *Maejo International Journal of Science and Technology* 10 (3), 313-329.
- [26] Janssen, H.A. (1895). *Versuche über Getreidedruck in Silozellen* (Texts on grain pressure in silos), Vereines deutscher Ingenieure, 39, 1045-1049. (partial English translation in proceedings of the Institute of Civil Engineers, London, England, 1896, P. 553.
- [27] Walker, D. M. (1966). An approximate theory for pressures and arching in hoppers. *Chemical Engineering Science*, 21(11), 975-97.
- [28] Walters, J. K. (1973a). A theoretical analysis of stresses in silos with vertical walls. *Chemical Engineering Science*, 28(1), 13-21.
- [29] Pipatpongsa, T., Khosravi, M. H., Wattanachai, P., and Likitlersuang, S. (2009). Stress Distributions in Storage Silo under Uniform Vertical Pressure. The 22th KKCNN Symposium on Civil Engineering, Chiang Mai, Thailand.
- [30] Pipatpongsa, T., Khosravi, M. H., and Heng, S. (2009). Granular arch shapes under criterion of silo effect. *Asian Pacific Conference for Materials and Mechanics*, The Japan Society of Mechanical Engineers, Yokohama, Japan.
- [31] Marston, A. and Anderson, A. O. (1913). The theory of loads on pipes in ditches and tests of cement and clay drain tile and sewer pipe. *Bulletins of the Engineering Experiment Station*, 31, 1-181.
- [32] Getzler, Z., Komornik, A., and Mazurik, A. (1968). Model study on arching above buried structures. *Journal of the Soil Mechanics and Foundations Division- ASCE*, 94(5), 1114-23.
- [33] Rankine, W. J. M. (1857). On the stability of loose earth. *Philosophical Transactions of the Royal Society of London*, 147, 9-27.
- [34] Krynine, D.P. (1945). Discussion of "Stability and stiffness of cellular cofferdams", *Transactions of the American Society of Civil Engineers* 10(1), 1175-1178.
- [35] Walters, J. K. (1973b). A theoretical analysis of stresses in axially-symmetric hoppers and bunkers. *Chemical Engineering Science*, 28(3), 779-89.
- [36] Coulomb, C. A. (1776). *Essai sur une application des règles de maximis & minimis à quelques problèmes de statique. relatifs à l'architecture. Mémoires de Mathématique et de Physique de l'Académie*, 7, 343-82.
- [37] Handy, R. L. (1985). The arch in soil arching. *Journal of Geotechnical Engineering- ASCE*, 111(3), 302-18.
- [38] Harrop-Williams, K. (1989). Geostatic wall pressures, *Journal of Geotechnical Engineering - ASCE* 115(9), 1321-1325.
- [39] Wang, Y. Z. (2000). Distribution of earth pressure on a retaining wall. *Geotechnique*, 50(1), 83-88.
- [40] Paik, K. H. and Salgado, R. (2003). Estimation of active earth pressure against rigid retaining walls considering arching effects. *Geotechnique*, 53(7), 643-53.
- [41] Khosravi, M. H. and Pipatpongsa, T. (2010). Arching effect in retaining walls under translation mode with surcharge. *The 45th National Conference of Japan Geotechnical Engineering*, Matsuyama, Japan.
- [42] Khosravi, M. H., Pipatpongsa, T., and Takemura, J. (2016). Theoretical analysis of earth pressure against rigid retaining walls under translation mode. *Soils and Foundations*, 56(4), 664-75.
- [43] Xie, Y. and Leshchinsky, B. (2016). Active Earth Pressures from a Log-Spiral Slip Surface with Arching. *Géotechnique Letters* 6 (2), 149-155.
- [44] Khosravi, M. H., Kargar, A. R. and Amini, M. (2018). Active earth pressures for non-planar to planar slip surfaces considering soil arching. *International Journal of Geotechnical Engineering*, DOI: 10.1080/19386362.2018.1503439.
- [45] Tsagareli, Z. V. (1965). Experimental investigation of the pressure of a loose medium on retaining walls with a vertical back face and horizontal backfill surface. *Soil Mechanics and Foundation Engineering*, 2(4), 197-200.
- [46] Sherif, M.A. and Fang, Y. (1984). Dynamic earth pressures on walls rotating about the top. *Soils and Foundations*, 24(4), 109-117.
- [47] Fang, Y. and Ishibashi, I. (1986). Static earth pressures with various wall movements. *Journal of Geotechnical Engineering- ASCE*, 112(3), 317-33.
- [48] Niedostatkiewicz, M., Lesniewska, D., and Tejchman, J. (2011). Experimental analysis of shear zone patterns in cohesionless for earth pressure problems using particle image velocimetry. *Strain*, 47(S2), 218-31.
- [49] Khosravi, M. H., Pipatpongsa, T., and Takemura, J. (2013). Experimental analysis of earth pressure against rigid retaining walls under translation mode. *Géotechnique*, 63(12), 1020-28.
- [50] Pipatpongsa, T., Khosravi, M. H., and Takemura, J. (2014). Physical model of a rigid retaining wall under translation mode and its variation of arch action in backfill material with interface friction. *The 8th International Conference on Physical Modelling in Geotechnics*, Perth, Australia.
- [51] Matsuzawa, H. and Hazarika, H. (1996). Analysis of active earth pressure against rigid retaining wall subjected to different modes of movement. *Soils and Foundations*, 36(3), 51-65.
- [52] Nadukuru, S. and Michalowski, R. (2012). Arching in distribution of active load on retaining walls. *Journal of Geotechnical and Geoenvironmental Engineering*, 138(5), 575-84.
- [53] Khosravi, M. H., Hamed Azad, F., Bahaaddini, M., and Pipatpongsa, T. (2017). DEM Analysis of Backfilled Walls Subjected to Active Translation Mode. *International Journal of Mining and Geo-Engineering* 51 (2), 191-197.
- [54] Jáky, J. (1948). Earth pressure in silos. *Proceedings of the 2nd International Conference on Soil Mechanics and Foundation Engineering*, ICSMFE1, 103-7